Simultaneous measurements of nitrate, oxygen and dissolved inorganic carbon on oceanographic moorings: Observing the Redfield Ratio in real-time

Kenneth S. Johnson, Monterey Bay Aquarium Research Institute, Moss Landing, California, USA

Abstract

The Redfield Ratio serves as a conceptual framework to link cycles of carbon, oxygen and nitrogen during respiration and photosynthesis in the ocean. Spatial variations in C:O:N ratios have been widely studied in the ocean and decadal scale variations in the ratios have also been examined. There are many fewer studies of these variations at high frequencies over time periods from daily to monthly. Here, autonomous measurements of dissolved nitrate, oxygen and total inorganic carbon (TCO_2 which is derived from pCO_2 and estimates of alkalinity) from sensors on the M1 and M2 moorings, off Monterey Bay, California are examined. Measurements were made from April to August 2006. These measurements are used to examine the linkages between nitrogen, oxygen and carbon cycling with the Redfield Ratio as a framework for the analysis. Concentrations of TCO_2, oxygen and nitrate were high pass filtered to remove low frequency changes driven by water mass changes. Daily cycles in each property are apparent with maxima or minima at the end of daylight that are consistent with biological production of oxygen or uptake of TCO_2 and nitrate. Ratio's of the changes in these diel cycles approach values expected from the Redfield values early in upwelling cycles. However, periods are frequently seen where the utilization of nitrate N is substantially lower than expected when compared to observed changes in TCO_2 or oxygen. During these periods, fixed nitrogen must be supplied from other sources such as ammonium or urea, or it is obtained by vertically migrating phytoplankton from deeper waters. These migrating phytoplankton must then return to the surface where inorganic carbon is consumed and oxygen is produced.

Acknowledgements

This work was supported by the David and Lucile Packard Foundation. Efforts of Gernot Friederich, Francisco Chavez, Luke Coletti, Carole Sakamoto, Mike Kelley, Paul Coenen and Mark Chaffey to support sensor deployments on the M1, M2 and MSE moorings are greatly appreciated.

Introduction

Redfield (1934) observed that the concentrations of dissolved nitrate, oxygen and inorganic carbon are present in the water and in plankton in nearly constant proportions. This observation has evolved towards an understanding that, on average, production or respiration of organic matter in the sea approximates the following equation:

$$106\ CO_2 + 16\ HNO_3 + 1H_3PO_4 + 122\ H_20 \leftrightarrow (CH_2O)_{106}\ (NH_3)_{16}\ H_3PO_4 + 138\ O_2 \qquad (1)$$

The stoichiometric ratio 106C:16N:1P:-138O_2 is termed the Redfield Ratio. This concept of closely linked elemental ratios in the biogeochemical cycles of the ocean has served as one of the foundations of biogeochemical research in the nearly 75 years since Redfield presented the concept (Falkowski, 2000). The oceanographic community has expanded on these concepts primarily by collecting samples in surveys that now span the global ocean and then measuring concentrations in these samples on board ship or on shore to examine the processes that regulate marine biogeochemistry. These results generally confirm the Redfield assessment, but have also led to revisions. For example, Anderson (1995) suggested that the oxygen coefficient be revised from -138 to -150. It is also clear that even the revised elemental ratio's are not fixed and abundant information on elemental cycling can be derived from anomalies relative to the mean values of the Redfield Ratio. Spatial variability in elemental ratios has been reported by Anderson and Sarmiento (1994) and Li and Peng (2002). Details of the spatial variability in nutrient ratio's have been used to estimate the global distribution of anthropogenic carbon

(Gruber and Sarmiento, 1997), nitrogen fixation (Deutsch et al., 2007), denitrification (Tyrell and Lucas, 2002) and ocean mixing (Broecker, 1974). There have been fewer studies of the variations in elemental ratio's in time. Temporal changes on decadal scale in the elemental ratios found near the euphotic zone (Karl et al., 2001) and in deep waters (Pahlow and Riebesell, 2000) have been discussed. Decadal scale changes in the Redfield Ratio are, however, difficult to detect, particularly in deep water, because of the long residence times of the chemicals (Keller et al., 2002). Seasonal changes in C:N ratio's have been noted in the North Atlantic, which appear to reflect overconsumption of N during rapid growth (Kortzinger et al., 2001). Although the community has gained greater insights, the processes that create the near constancy in elemental ratio's continue to be examined (Lenton and Watson, 2000; Klausmeier et al., 2004).

It is now possible to measure nitrate (Johnson and Coletti, 2002; Johnson et al., 2006; Kortzinger et al., 2008a), oxygen (Tengberg et al., 2006; Kortzinger et al., 2008b) and pCO2 (Friederich et al., 1995; Friederich et al., 2002; Kortzinger et al., 2008a; 2008b; Hood and Merlivat, 2001) on oceanographic moorings for year-long periods of time without substantial degradation in sensor performance. Each of these chemicals is closely linked through Eq. (1) to the primary production and respiration of organic carbon. For example, it has been demonstrated that diel cycles in concentration of nitrate can be used to provide near-daily estimates of primary production for sustained (years) periods (Johnson et al., 2006). Diel variations in oxygen and inorganic carbon are also used to examine temporal changes in primary productivity (Odum, 1958; Yates et al., 2007). The capacity for long-term, autonomous

observations of multiple chemicals now allows the linkages between chemical cycles to be monitored continuously (Johnson et al., 2007).

Here, I examine measurements of nitrate, oxygen and inorganic that were reported by in situ sensors on the M1 and M2 moorings offshore of Monterey Bay, California. These are highly instrumented moorings (Chavez et al., 1997) that have been maintained since 1989. Measurements of ΔpCO_2, the difference in sea and air pCO_2, have been made since 1993 on these moorings (Friederich et al., 1995). These measurements have been used to examine long-term changes in air-sea gas exchange of CO_2 driven by processes such as El Nino (Friederich et al., 2002). Measurements of nitrate concentration on the moorings began in 2002 using optical nitrate sensors (Johnson and Coletti, 2002). These measurements have been used to examine daily to annual changes in primary production (Johnson et al., 2006). Dissolved oxygen measurements using the Aanderaa Optode systems (Tengberg et al., 2006) became operational on both moorings in April 2006. This paper uses the Redfield model as a framework to interpret the daily variations in the ratio's of total dissolved inorganic carbon (TCO_2), whose concentration is inferred from pCO_2, dissolved oxygen and nitrate. The analysis focuses on the period from April 2006 through August 2006. However, these measurements all continue, with some interruptions, through the present. The data are delivered to the Internet at several web pages located at http://www.mbari.org where they are available for analysis by the community.

Methods

The M1 and M2 mooring locations are 36.747° N, 122.022° W (1200 m depth) and 36.697°N, 122.378° W (1800 m depth) offshore of Monterey Bay (Fig. 1). These moorings are 20 and 50 km offshore, respectively. In addition, some data collected at the MSE mooring are shown. It was located at 36.2°N, 122.9°W (3300 m depth), which is 115 km offshore..

Nitrate was measured at 1 m depth using ISUS nitrate sensors (Johnson and Coletti, 2002). The mooring data, including the complete ultra-violet spectrum measured by ISUS, are transmitted to shore hourly. Nitrate concentrations are calculated using the measured light absorption spectrum from 217 to 240 nm and a linear baseline estimate. Biofouling of the optics was inhibited with a copper anti-fouling shield. The ISUS sensor calculates nitrate concentration using the algorithm described in Johnson and Coletti (2002). A revised algorithm that substantially improves the accuracy of UV nitrate measurements has been developed (Sakamoto et al., 2009). All of the data reported here were reprocessed with that new algorithm. This involves correcting the bromide molar absorptivities to the in situ temperature. The salinity measured with the CTD is then used to predict bromide ion concentration using the known bromide to chlorinity ratio (Morris and Riley, 1966) and the temperature corrected bromide molar absorptivities are used to calculate the UV spectrum due to bromide. This bromide spectrum is subtracted from the observed UV spectrum. Nitrate is determined by fitting the bromide corrected sea water spectra with the molar absorptivities of nitrate, which are temperature independent, and an absorbance baseline that is a linear function of wavelength.

The accuracy of nitrate concentrations calculated with the revised algorithm is significantly improved relative to the original algorithm, as shown by an extensive set of comparisons between sensor data and nitrate measurements made in the laboratory (Sakamoto et al., 2009). In relatively clear water, such as that found in Monterey Bay and with little fouling of the sensor, which is achieved in the AUV by rinsing the optics before each mission, concentrations computed with the revised algorithm should be accurate to <1 μmol L^{-1} nitrate.

The pCO_2 difference between seawater and air ($\Delta pCO_2 = pCO_{2,\,SW} - pCO_{2,\,Air}$) was measured as described in Friederich et al., (1995; 2002). The $pCO_{2,\,SW}$ was estimated from ΔpCO_2 by assuming that $pCO_{2,\,Air}$ was constant at 380 μatm. Titration alkalinity (TA) was estimated from the observed salinity and temperature (Lee et al., 2006). TCO_2 was then calculated using the CO2SYS_MACRO_PC Excel spreadsheet program (Pierrot et al., 2006) with the observed T and S and the estimates of $pCO_{2,\,SW}$ and TA as inputs. Oxygen was measured with an Aanderaa Oxygen Optode (Tengberg et al., 2006) at 1 m depth. The Optode measures oxygen partial pressure and the in situ salinity and temperature were used to compute oxygen concentration using algorithms supplied by Aanderaa. The Optode was protected from fouling with a copper mesh pad as suggested by the manufacturer. Chlorophyll fluorescence was measured with a WetLabs WetStar fluorometer on each mooring. Temperature and Salinity were measured with SeaBird Model 37 conductivity, temperature and depth (CTD) sensors.

Results and Discussion

The results for temperature and salinity on the M1 and M2 moorings are shown in Figure 2. Daily average chlorophyll and hourly values of nitrate, oxygen and total inorganic carbon concentrations are shown in Figure 3. Chlorophyll was binned to daily averages because of the large diurnal cycle produced by daytime fluorescence quenching (Falkowski and Kiefer, 1985). In principle, nighttime values of chlorophyll fluorescence are most useful, but most samples near the moorings are collected during the day when quenching is most severe. Daily averages are used here, as a compromise. To assess the accuracy of the chemical data, concentrations of nitrate, oxygen and TCO_2 measured in the NE Pacific during the World Ocean Circulation Experiment (WOCE) are superimposed on Figures 4a and 4c. The WOCE data were obtained from the eWOCE electronic atlas (Schlitzer, 2000) by extracting all oxygen, TCO_2 and nitrate data from the upper 200 m and collected within the box bounded by 30 to 39°N, 138 to 118°W. All concentrations were converted from mol kg^{-1} to mol l^{-1} units and TCO_2 was normalized to a salinity of 33.4, typical of the values observed at the moorings. Agreement between the nitrate and TCO_2 data estimated for the mooring and the WOCE observations (Fig. 4c) is reasonable. The mooring oxygen data (Fig. 4a) have a higher range than do the WOCE data at similar values of total inorganic carbon. This is likely a result of very high rates of primary production in coastal waters that create oxygen faster than outgassing can remove it. Primary production creates oxygen concentrations that exceed atmospheric equilibrium values by as much as 150% (Fig. 5). The surface oxygen concentrations in the WOCE data, which are all from lower

productivity offshore waters, remain near 100% of the atmospheric equilibrium values due to low rates of primary production in offshore waters and rapid outgassing of dissolved oxygen. Air-sea gas exchange has a much slower impact on TCO_2 because of the dissociation of carbonic acid and gas exchange does not appear to bias the comparison of mooring and WOCE data.

Much of the variability in properties seen in Figures 2 and 3 is created by a sequence of upwelling events that bring cold, salty, nutrient-rich water to the surface. During upwelling events, the M1 mooring lies directly in the path of an upwelled plume of water that originates near Point Año Nuevo, to the north of Monterey Bay (Rosenfeld et al., 1994; Breaker and Broenkow, 1994; Fitzwater et al., 2003). In strong upwelling events, the plume reaches the M2 mooring about 1 day after reaching M1. The temporal patterns in temperature at M1 and M2 are generally similar. There is one upwelling event at M1 in late May and early June which, apparently, did not reach M2 as there is no corresponding temperature or salinity signal (Figure 2).

These upwelling events lead to large changes in chemical concentrations (Figure 3). During these events, concentrations of nitrate, oxygen and total inorganic carbon are highly correlated at each mooring (Figure 4). These correlations are driven by both physical mixing of waters with different properties and by in situ production or respiration of fixed organic carbon. The effects of physical and biological processes on bulk chemical concentrations are difficult to separate in this dynamic environment because both have similar signatures. Upwelled waters are enriched in nitrate and TCO_2 and depleted in oxygen as a result of respiration of organic matter.

This produces chemical concentrations that are highly correlated when deep water mixes with surface waters. The same signals are produced by local uptake of nitrate and inorganic carbon and production of oxygen during daily photosynthesis and respiration cycles.

One line of evidence that points to high local rates of primary production is the high degree of oxygen saturation. The oxygen concentration reaches values well above saturation with respect to atmospheric oxygen. Percent saturation of oxygen is as high as 160% (Figure 5). Local heating can also create supersaturation, but temperature changes of more than 20 °C would be required to change saturation by 160%. Local heating appears to change temperature by less than 5°C. The high percent saturation implies that local rates of primary production must be an important process in controlling surface oxygen concentration.

Diel cycles in nitrate concentration are regularly observed with in situ sensors (Johnson et al., 2006). These cycles are produced by nitrate uptake during daylight and resupply during the dark. The daily cycle can be used as a quantitative metric of net primary production (Johnson et al., 2006). This analysis of diel patterns involves high pass filtering the data so that only signals with a period shorter than 33 hours remain in the data set. The high pass filter removes low frequency changes in the data that might result from mixing of multiple water masses. In the following section, the data sets that result after applying a high pass filter to all of the chemical measurements are examined.

High Pass Filtered Chemical Concentrations.

The high pass filtered concentrations of nitrate, oxygen and TCO_2 at the M1 mooring are shown in Fig. 6. The changes in each chemical concentration are highly correlated (Fig. 7). The amplitude of changes in nitrate are about one tenth of the values observed for oxygen and TCO_2. However, the slopes of the high pass filtered property-property plots, which were determined from Model II linear regressions to account for errors in each variable (Laws, 1997), are significantly different than the values expected from the Redfield Ratio (Table 1).

The discrepancy in the O_2:TCO_2 slope at both moorings, relative to the Redfield value, can likely be explained by the effects of gas exchange. A piston velocity of 2 m d^{-1} (10 cm h^{-1}) is a typical gas exchange rate constant at modest wind speeds (Wanninkhof et al., 2009). Air-sea gas exchange at this rate would remove 20 to 40% of the oxygen saturation anomaly on a daily basis with a mixed layer depth of 5 to 10 m, typical of the spring and summer near M1. The rate of air-sea gas exchange for TCO_2 will be about 10x lower due to the reaction of carbon dioxide with carbonate ion and it will be relatively unaffected by gas exchange over the same time period. As a result, gas exchange will bias the oxygen anomalies low, relative to the Redfield value, by about the amount shown in Table 1. If the O_2:TCO_2 ratio suggested by Anderson (1995) were used, rather than Redfield, the anomalies would be larger, but still explainable by gas exchange processes.

To understand the reasons for the discrepancies in the observed NO_3^-:TCO_2 or NO_3^-:O_2 slopes, relative to the Redfield value, it is necessary to examine the data more closely. Fig. 8

212 shows one example of the unfiltered and filtered chemistry data at the M1 mooring for the period
213 from July 9 to July 16. The plot of the high-pass filtered data has been scaled using the Redfield
214 Ratio (oxygen and TCO_2 anomaly ranges are the same) so that a concentration change in each
215 property that follows Eq. 1 would span the same vertical range. Concentration changes driven
216 by photosynthesis are oriented up (ie., the concentration scale for O_2 has the opposite sign as for
217 NO_3^- and TCO_2). The dotted vertical lines mark the end of each day in GMT, which corresponds
218 to 1700 local time and is near the end of daylight. The example shown in Fig. 8 shows behavior
219 that is typical of much of the data set. The plot begins during a period of strong, upwelling
220 favorable winds that have brought cold, nitrate-rich water to the surface. Chlorophyll
221 concentrations (Fig. 8c) are low in the freshly upwelled water. The wind began to weaken on
222 July 10 and chlorophyll concentrations increased rapidly. As chlorophyll increases, diel cycles
223 develop in nitrate, oxygen and TCO_2 that scale closely to the values expected from the Redfield
224 Ratio (Fig. 8b). The NO_3^-:TCO_2 ratio during this period is 0.12±0.01 (13:106), somewhat closer
225 to the Redfield value than the overall mean value of 0.073±0.002 (7.7:106) at M1.
226 Figure 9 shows the chemical concentrations and their high-pass filtered values during a
227 subsequent period from July 21 to July 30. Nitrate concentrations drop to low values near 1 μM
228 on July 25 and remain low for several days. Although nitrate concentration is low and its diel
229 cycle is very small after the July 25, the diel cycles of TCO_2 and oxygen continue with large
230 amplitudes. The large diel cycles in both TCO_2 and oxygen are unlikely to be the result of
231 sensor fouling, as the two systems are completely independent. The NO_3^-:TCO_2 ratio is

232 0.021±0.007 (2.2:106) for July 25 to 28 and 0.076±0.008 (8:106) for the period July 21 to July
233 30. There is nearly complete decoupling of nitrate from the carbon and oxygen cycles for three
234 days and the mean ratio for the entire period is about one half of the Redfield value. Such
235 decoupling of nitrate from oxygen and carbon cycling is apparent for short periods throughout
236 the data set. This leads to the low value of the NO_3^-:TCO_2 ratio for the entire data set.
237 The concentration of chlorophyll increases during this period with low nitrate (Fig. 9c)
238 indicating that there is net production of organic matter. There are multiple reasons why nitrate
239 might be decoupled from the oxygen and TCO_2 cycles while organic carbon is produced. Other
240 sources of fixed nitrogen, such as ammonia or urea, might fuel production of organic matter.
241 Alternatively, a population consisting of dinoflagellates might be capable of migrating vertically
242 to the nitracline to acquire nitrate and then return to the surface where photosynthesis takes
243 place. These two processes cannot be resolved with the data that are available, but it would
244 certainly be feasible to instrument moorings to put further constraints on these processes. For
245 example, it is now possible to measure dissolved ammonia on moorings in a nearly routine
246 manner (Plant et al., 2009).
247
248 Biomass Production
249 Daily estimates of net production of organic matter were calculated from the amplitude of
250 the high-pass filtered concentrations. To calculate the amplitude, the minimum values of high-
251 pass filtered nitrate and TCO_2 (maximum for oxygen) were found each day for the period from

2200 to 0300 GMT (1500 to 2000 PDT) and the mean concentration for the three hour period centered on that time was calculated. Maximum values (minimum for oxygen) were found each day between 1100 to 1600 GMT (0400 to 0900 PDT) and the mean concentration for the three hour period centered on that time was again calculated. The diel amplitude due to primary production was set as the difference of these two values for each chemical. These diel amplitudes for nitrate and oxygen were then converted to carbon units using the Redfield Ratio. The results are shown in Fig. 10 for M1 and M2.

Each of the daily amplitudes of the high-pass filtered nitrate, oxygen and TCO_2 concentrations is an independent estimate of the net production of organic matter (Johnson et al., 2006). TCO_2 and, to a lesser extent, O_2 based production values are larger than the nitrate based production estimates (Fig. 10). There is also one example (M2, mid- to late-July; Fig. 10) where oxygen amplitude is high and the carbon and nitrate amplitudes are much lower. This may reflect fouling of the oxygen sensor, although it began returning values consistent with its early performance without any cleaning.

The daily estimates of new production can be used to predict the accumulation of biomass using the equation (Johnson et al., 2006):

$$B_t = B_{t-1} + \Delta_t \times NCP - \Delta_t \times L \times B_{t-1} \qquad (2)$$

where B is biomass in carbon units, NCP is the daily estimate of net community production of carbon derived from the diel amplitude of nitrate, oxygen or TCO_2 measurements (Fig. 10), and Δ_t is a one hour time step. L is the rate constant for loss of biomass due to all factors including grazing, sinking, and removal by horizontal advection. The amplitude of the nitrate diel cycle is a reflection of net production that incorporates dissolved nitrate from surface waters, while the amplitudes of oxygen and TCO_2 would reflect production from all fixed nitrogen sources. Integration of Eq. 2 was begun with an initial biomass value of zero.

The biomass values calculated using NCP derived from the TCO_2 concentrations are shown in Fig. 11 for M1 and M2. Carbon biomass was converted to chlorophyll units using a constant C:chlorophyll ratio (by weight) of 60 (Johnson et al., 2006). L is not constrained directly by the chemical observations. It was, therefore, adjusted by comparing the predicted chlorophyll with the values observed at each mooring and minimizing the sum of the squared errors. A value of 0.6 d^{-1} is near the optimum at both M1 and M2 and that value has been used to compute the predicted chlorophyll concentrations shown in Fig. 11. The estimates of chlorophyll that are derived from NCP values based on the diel cycle of TCO_2 are in good agreement with the observed, daily mean values of chlorophyll with an $R^2 = 0.45$ at M1 and $R^2 = 0.25$ at M2. The predicted chlorophyll values capture nearly all of the major bloom cycles seen at both moorings (Fig. 11). These results demonstrate that it is possible to use in situ chemical observations to determine how much carbon is produced each day and, with a single adjustable

parameter that relates to biomass loss, to also predict the temporal course of biomass standing stocks over periods of multiple months.

Similar results for biomass standing stocks are found using the high pass filtered data for dissolved oxygen when it is converted to carbon units using the Redfield Ratio. For example, the R^2 between chlorophyll modeled with productivity based on oxygen daily amplitude and observed values is 0.48 at M1. However, the time course of biomass predicted using high pass filtered nitrate concentrations is somewhat different for the period of this study. The modeled chlorophyll values determined using TCO_2 and nitrate, after conversion to carbon equivalents using the Redfield Ratio, are plotted versus each other in Fig. 12. While the two values are highly correlated ($R^2 = 0.47$), the slope of a line fitted to all of the data is 0.45, rather than the expected value of 1. If the value of L is optimized using growth rates based on nitrate, the best fit value is 0.33 d^{-1}, rather than 0.6 d^{-1} when TCO2 daily amplitudes are used. The diel cycles based on nitrate concentrations predict, on average, only about one half of the biomass accumulation predicted from TCO_2 cycles. Presumably, the remainder of the biomass accumulation is derived from fixed nitrogen sources other than the nitrate that is found in surface waters. These sources might include ammonium or vertical migration to obtain nitrate at greater depths.

Figure 13 shows the sequence of events during an upwelling period in May 2006 at the M2 mooring. Nitrate concentrations increase from near zero values to 12 μM in two main pulses. TCO_2 increases in parallel with nitrate and it clearly shows diel cycles with minima at

sunset on most days. Growth rates based on diel amplitudes of TCO_2 and NO_3^- increase within the nutrient rich, upwelled water from near zero values before onset of the upwelling event. As growth rates increase, both the modeled and observed chlorophyll concentrations increase at similar rates. Observed chlorophyll and values modeled using TCO_2 diel cycles continue to increase while dissolved nitrate is present to fuel growth. The chlorophyll concentration declines in late May, as nitrate is depleted. The growth rates based on nitrate track the values based on TCO_2 near the beginning of the upwelling period. However, as biomass increases, the growth rates based on TCO_2 exceed those based on nitrate. Either the phytoplankton are growing with C:N ratio's that are nearly double the Redfield value, or recycled nitrogen in the form of ammonia is also serving as a significant N source.

Limits of detection

In order to assess the lower limits of production at which diel chemical cycles can be detected, oxygen sensor data from the MSE mooring, which was deployed at 115 km off the coast, is considered. High-pass filtered oxygen data from M1, M2 and MSE from November 2006 to May 2007 are shown in Fig. 14 a-c. One large gap in the MSE data occurred when the sensor fouled, which was diagnosed as a rapid increase in diel amplitude, followed by a drop to near zero oxygen concentration. After the sensor was cleaned and the anti-fouling copper mesh was replaced, the sensor began to return measurements similar to values observed before the

fouling event. Clear diel cycles with maxima near the end of daylight are seen at the MSE mooring, as well as at M1 and M2, throughout this period (Fig. 14 d-e). The mean values of the diel amplitude for the November to May period are shown in Fig. 15a as a function of distance from the coast and as a histogram diel amplitude observed at each mooring is shown Fig. 15 b-d. The amplitude at the MSE mooring (2.2± 0.4 mmol O_2 m^{-3} d^{-1}, 95% CI) is a factor of 5 lower than at M1 and M2 and it is easily resolved during this period. A lower limit to reliably detection is probably around 0.5 to 1 mmol O_2 m^{-3} d^{-1}.

In conclusion, the results shown here demonstrate that the daily cycles of inorganic carbon, oxygen and nitrate are often closely coupled in ratios near those expected from Redfield (Eq. 1). However, there is also significant decoupling of the observed parameters over short time periods. This is particularly true for the C:N ratio. Because only nitrate was sensed, which is one of many possible forms of fixed nitrogen, this decoupling does not demonstrate that organic matter is produced with distinctly non-Redfieldian composition. Rather, it most likely indicates that, even in dynamic, coastal upwelling ecosystems, nitrate present in surface waters is not always the dominant fixed nitrogen source for phytoplankton. In Monterey Bay, only about one half of the required nitrogen appears to be supplied directly from surface waters during the time of this study.

347 References

348 Anderson, L. A. 1995. On the hydrogen and oxygen content of marine phytoplankton. Deep-
349 Sea Res. I 42: 1675-1680.

350 Anderson, L. A. and J. L. Sarmiento. 1994. Redfield ratios of remineralization determined by
351 nutrient data analysis. Global Biogeochem. Cycles 8: 65-80.

352 Breaker, L.C., and W. W. Broenkow. 1994. The circulation of Monterey Bay and related
353 processes. Oceanogr. Mar. Biol. Annu. Rev. 32: 1–64.

354 Broecker, W. S. 1974. "NO" a conservative water-mass tracer. Earth Planet. Sci. Lett. 23: 100-
355 107.

356 Chavez, F. P., J. T. Pennington, R. Herlien, H. Jannasch, G.Thurmond, and G. E. Friederich.
357 1997. Moorings and drifters for real-time interdisciplinary oceanography. J. Atm. Ocean.
358 Tech. 14: 1199–1211.

359 Deutsch, C., J. L. Sarmiento, D. M. Sigman, N. Gruber, and J. P. Dunne. 2007. Spatial coupling
360 of nitrogen inputs and losses in the ocean. Nature 445: 163-167.

361 Falkowski, P. G. 2000. Rationalizing elemental ratios in unicellular algae. J. Phycol. 36: 3-6.

362 Falkowski, P. G. and D. A. Kiefer. 1985. Chlorophyll a fluorescence in phytoplankton:
363 relationship to photosynthesis and biomass. J. Plankton Res. 7: 715-731.

364 Fitzwater, S. E., K. S. Johnson, V. A. Elrod, J. P. Ryan, L. J. Coletti, S. J. Tanner, R. M. Gordon,
365 and F. P. Chavez. 2003. Iron, nutrient and phytoplankton biomass relationships in
366 upwelled waters of the California coastal system. Cont. Shelf Res. 23: 1523-1544.

Friederich, G. E., P. G. Brewer, R. Herlien, and F. P. Chavez. 1995. Measurements of sea surface partial pressure of CO2 from a moored buoy. Deep-Sea Res. I 42: 1175–1186.

Friederich, G. E., P. M. Walz, M. G. Burczynski, and F. P. Chavez. 2002. Inorganic carbon in the central California upwelling system during the 1997–1999 El Nino–La Nina event Progr. Oceanogr. 54: 185-203.

Gruber, N. and J. L. Sarmiento. 1997. Global patterns of marine nitrogen fixation and denitrification. Glob. Biogeochem. Cycles 11: 235–266.

Hood, E. M., and L. Merlivat. 2001. Annual to interannual variations of fCO2 in the northwestern Mediterranean Sea: Results from hourly measurements made by CARIOCA buoys, 1995–1997. J. Mar. Res. 59: 113-131.

Johnson, K. S., and L. J. Coletti. 2002. In situ ultraviolet spectrophotometry for high resolution and long term monitoring of nitrate, bromide and bisulfide in the ocean. Deep-Sea Res. I 49: 1291-1305.

Johnson, K. S., L. J. Coletti, and F. P. Chavez. 2006. Diel nitrate cycles observed with in situ sensors predict monthly and annual new production. Deep-Sea Res. I 53: 561-573.

Johnson, K. S., J. A. Needoba, S. C. Riser, and W. J. Showers. 2007. Chemical sensor networks for the aquatic environment. Chem. Rev. 107: 623-640.

Karl, D. M., K. M. Bjorkman, J. E. Dore, L. Fujieki, D. V. Hebel, T. Houlihan, R. M. Leterlier, and L. M. Tupas. 2001. Ecological nitrogen-to-phosphorous stoichiometry at station ALOHA. Deep-Sea Res. II 48: 1529-1566.

Keller, K., R. D. Slater, M. Bender, and R. M. Key. 2002. Possible biological or physical explanations for decadal scale trends in North Pacific nutrient concentrations and oxygen utilization. Deep-Sea Res. 49: 345-362.

Klausmeier, C. A., E. Lichman, T. Daufresne, and S. A. Levin. 2004. Optimal nitrogen-to-phosphorous stoichiometry of phytoplankton. Nature 429: 171-174.

Kortzinger, A., W. Koeve, P. Kahler, and L. Mintrop. 2001. C:N ratios in the mixed layer during the productive season in the northeast Atlantic Ocean, Deep Sea Res., Part I 48: 661– 688.

Kortzinger, A., and others. 2008a. The seasonal pCO_2 cycle at 49°N/16.5°W in the northeastern Atlantic Ocean and what it tells us about biological productivity. J. Geophys. Res. 113: C04020, doi:10.1029/2007JC004347.

Kortzinger, A., U. Send, D. W. R. Wallace, J. Karsten, and M. DeGrandpre. 2008b. Seasonal cycle of O_2 and pCO_2 in the central Labrador Sea: Atmospheric, biological, and physical implications. Global Biogeochem. Cycles 22, GB1014, doi:10.1029/2007GB003029.

Laws, E. A. 1997. Mathematical Methods for Oceanographers: An Introduction. Wiley-Interscience.

Lee, K., and others. 2006. Global relationships of total alkalinity with salinity and temperature in surface waters of the world's oceans. Geophys. Res. Lett. 33: L19605, doi:10.1029/2006GL027207.

Lenton, T. M., and A. J. Watson. 2000. Redfield revisited 1. Regulation of nitrate, phosphate, and oxygen in the ocean. Global Biogeochem. Cycles 14: 225–248.

Li, Y.-H., and T.-H. Peng. 2002. Latitudinal change of remineralization ratios in the oceans and its implication for nutrient cycles. Global Biogeochem. Cycles 16: 1130, doi:10.1029/2001GB001828.

Morris, A. W., and J. P. Riley. 1966. The bromide/chlorinity and sulphate/chlorinity ratio in sea water. Deep-Sea Res. 13: 699-705.

Odum, H. T. 1956. Primary production in flowing waters. Limnol. Oceanogr. 1: 102-117.

Pahlow, M., and U. Riebesell. 2000. Temporal trends in deep ocean Redfield ratios. Science 287: 831–833.

Pierrot, D., E. Lewis, and D. W. R. Wallace. 2006. MS Excel Program Developed for CO2 System Calculations. ORNL/CDIAC-105. Carbon Dioxide Information Analysis Center, Oak Ridge National Laboratory, U.S. Department of Energy, Oak Ridge, Tennessee.

Plant, J. N., K. S. Johnson, J. A. Needoba, and L. J. Coletti. 2009. NH4-Digiscan: an in situ and laboratory ammonium analyzer for estuarine, coastal and shelf waters. Limnol. Oceanogr.: Methods 7: 144-156.

Redfield, A. C. 1934. On the proportions of organic derivatives in sea water and their relation to the composition of plankton, p. 177-92. In: R. J. Daniel [ed.], James Johnstone Memorial Volume. University Press of Liverpool.

Rosenfeld, L. K., F. B. Schwing, N. Garfield, and D. E. Tracy. 1994. Bifurcated flow from an upwelling center: a cold water source for Monterey Bay. Cont. Shelf Res. 14: 931-964.

426 Sakamoto, C. M., K. S. Johnson and L. J. Coletti. 2009. An improved algorithm for the
427 computation of nitrate concentrations in seawater using an in situ ultraviolet
428 spectrophotometer. Limnol. Oceanogr.: Methods 7: 132-143.
429 Schlitzer, R. 2000. Electronic atlas of WOCE hydrographic and tracer data now available. Eos
430 Trans. Am. Geophys. Union 81:, 45.
431 Tengberg, A., and others. 2006. Evaluation of a lifetime-based optode to measure oxygen in
432 aquatic systems. Limnol. Oceanogr.: Methods 4: 7-17.
433 Tyrrell, T., and M. I. Lucas. 2002. Geochemical evidence of denitrification in the Benguela
434 upwelling system. Cont. Shelf Res. 22: 2497-2511.
435 Wanninhkof, R., W. E. Asher, D. T. Ho, C. S. Sweeney, and W. R. McGillis. 2009. Advances
436 in quantifying air-sea gas exchange and environmental forcing. Annu. Rev. Mar. Sci. 1:
437 213-244.
438 Yates, K. K., C. Dufore, N. Smiley, C. Jackson, and R. B. Halley. 2007. Diurnal variation of
439 oxygen and carbonate system parameters in Tampa Bay and Florida Bay. Mar. Chem.
440 104: 110-124.

Table 1. Ratio's of high pass filtered chemical anomalies at the M1 and M2 moorings estimated from data in Figure 7 using a Model II regression (Laws, 1997). 95% confidence limits for the ratio are shown.

Ratio	Redfield	M1	M2
NO_3^-:TCO_2	0.15 (16:106)	0.073±0.002 (7.7:106)	0.071±0.002 (7.5:106)
NO_3^-:O_2	-0.12 (16:138)	-0.095±0.003 (13:138)	-0.076±0.002 (10:138)
O_2:TCO_2	-1.30 (138:106)	-0.77±0.02 (81:106)	-0.93±0.03 (98:106)

441 Figure Legends

442

443 Figure 1. Mooring locations offshore of Monterey Bay, California. Depth contours in
444 meters.

445

446 Figure 2. Temperature (a) and salinity (b) at the M1 and M2 moorings.

447

448 Figure 3. Daily mean values of chlorophyll at the M1 (a) and M2 (b) moorings. Hourly
449 values of nitrate (c, d), dissolved oxygen (e, f) and TCO_2 (g, h) at M1 and M2.

450

451 Figure 4. Dissolved oxygen is plotted versus TCO2 at the M1 (a) and M2 (b) moorings.
452 Nitrate is plotted versus TCO2 at the M1 (a) and M2 (b) moorings. Red dots in (a) and (c) show
453 near surface values for the same parameters in the NE Pacific obtained during the WOCE
454 program (Schlitzer, 2000).

455

456 Figure 5. Oxygen percent saturation with respect to atmospheric solubility at the M1
457 (black line) and M2 (red line) moorings.

458

459 Figure 6. High pass filtered concentrations of nitrate (a), oxygen (b) and TCO_2 (c) at the
460 M1 mooring.

Figure 7. High pass filtered concentrations of nitrate (a) and TCO_2 (b) vs. high pass filtered concentration of oxygen and the high pass filtered concentration of nitrate vs. high pass filtered concentration of TCO_2 (c) at the M1 mooring. Panels d, e and f are the same for the M2 mooring. Red lines are Model II regression lines fitted to the data. Slopes of the regressions are shown in each panel.

Figure 8. Concentrations of nitrate (black line), oxygen (red line) and -1 x TCO2 (green line) from 7/9/2006 to 7/16/2006 (a). High pass filtered concentrations of the same properties are shown in (b). The axes for each property are scaled to span a similar range when normalized to the Redfield Ratio and each scale is oriented so that changes driven by uptake during primary production are oriented up. Daily average estimates of chlorophyll are shown in (c) for the same period. Time is GMT and local sunset is near 0300.

Figure 9. As in Figure 8 for the period 7/21/2006 to 7/30/2006.

Figure 10. Diel amplitude of the high-pass filtered nitrate (black line), oxygen (red line) and TCO_2 (green line) at the M1 mooring (a) and M2 mooring (b).

Figure 11. Observed chlorophyll concentrations (solid lines) and values computed from Eq. (2) using net community production values estimated from the TCO_2 diel amplitude (dashed lines) are shown for the M1 mooring (a) and the M2 mooring (b). A single high value of the TCO_2 diel amplitude, which was observed on 5/21/2006 (128 mmol C m^{-3} d^{-1}) and which is offscale in Figure 10, was replaced by the average of the two adjacent values for the model calculations.

Figure 12. Chlorophyll computed from Eq. (2) using diel amplitudes derived from nitrate observations are plotted versus chlorophyll computed from Eq. (2) using TCO_2 diel amplitudes. The dashed line is a Model II regression with slope 0.45±0.06 (95% CI). The solid line has slope 1.

Figure 13. Nitrate (dashed line) and TCO_2 (solid line) concentrations observed at the M2 mooring from 5/1/2006 to 6/5/2006 (a). Diel amplitudes of nitrate, after conversion to carbon units using the Redfield Ratio (dashed line) and TCO_2 (solid line) are shown for the same time period (b). Observed daily mean chlorophyll values (solid line) and values computed from Eq. 2 using the diel amplitudes derived from TCO_2 (dashed line) are shown for the same time period (c).

Figure 14. High-pass filtred oxygen concentrations from 11/1/2006 to 5/10/2007 (a) and 1/10/2007 to 1/20/2007 (b) at the M1 mooring. Panels (c) and (d) are the same at the M2 mooring. Panels (e) and (f) are the same at the MSE mooring.

Figure 15. Mean diel oxygen amplitudes at M1, M2 and MSE versus distance from Moss Landing (a). Error bars are 95% confidence intervals. Histograms of the diel oxygen amplitudes at M1 (b), M2 (c) and MSE (d) are also shown. The mean and 95% confidence intervals are shown on each panel.

507 Figure 1

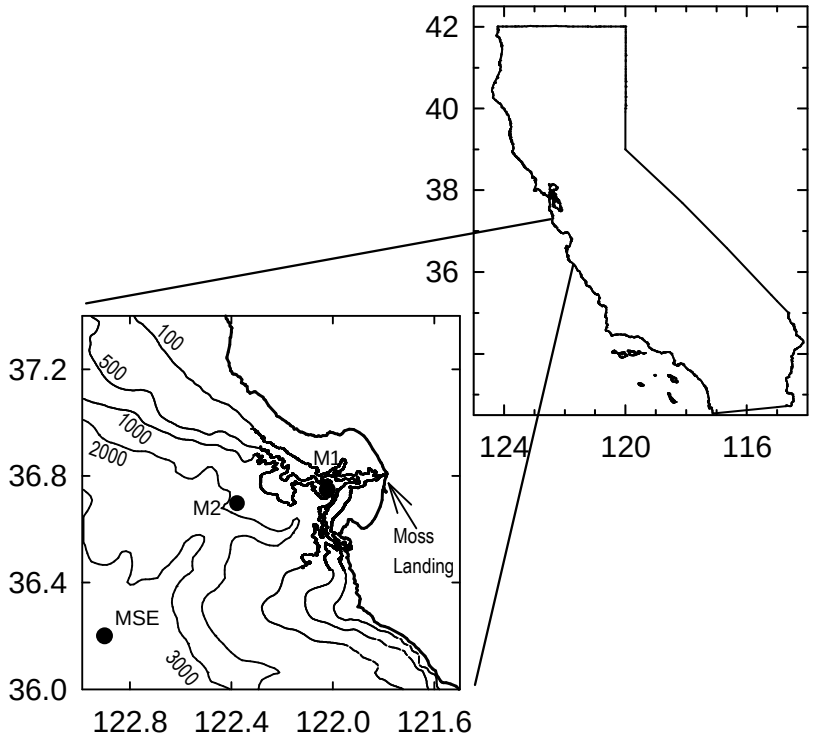
42
40
38
36
124
120
116
37.2
36.8
36.4
36.0
122.8
122.4
122.0
121.6
100
500
1000
2000
3000
M1
M2
MSE
Moss
Landing

508 Figure 2

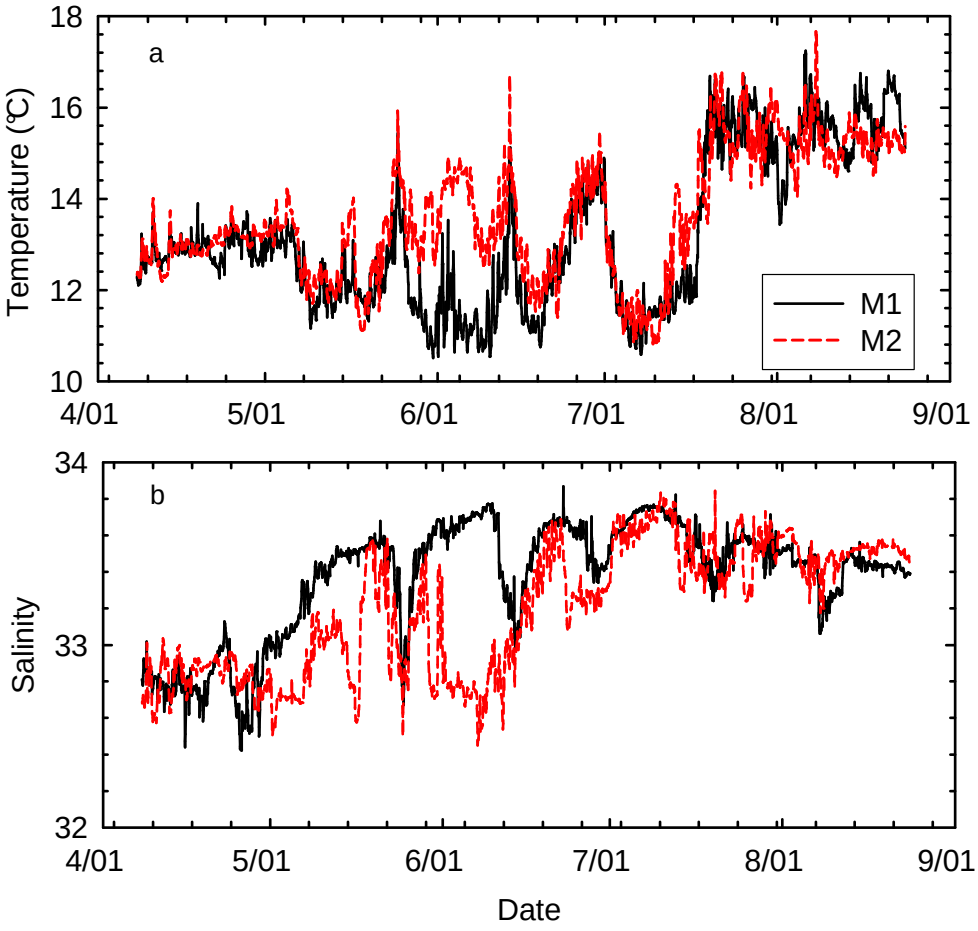
a
b
Temperature (℃)
Salinity
M1
M2
18
16
14
12
10
34
33
32
4/01
5/01
6/01
7/01
8/01
9/01
Date

509 Figure 3

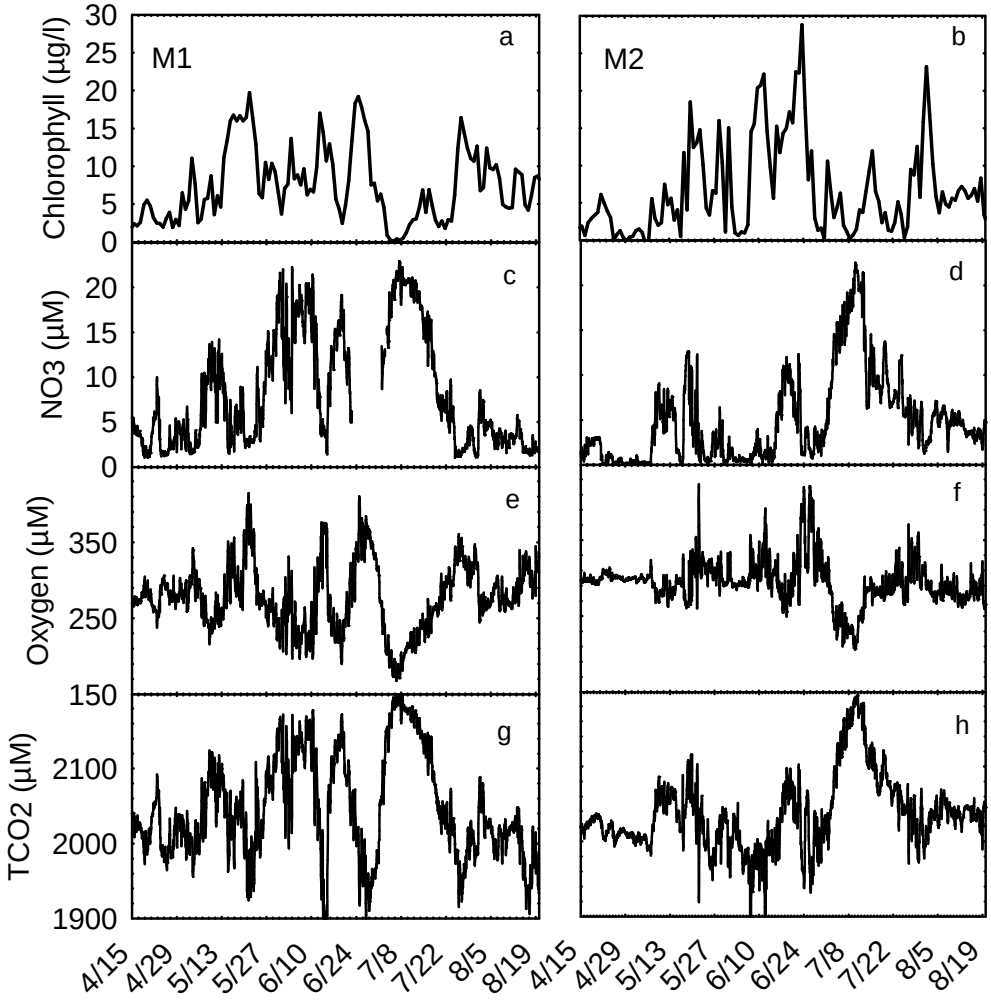
M1
M2
a
b
c
d
e
f
g
h
Chlorophyll (µg/l)
NO3 (µM)
Oxygen (µM)
TCO2 (µM)
30
25
20
15
10
5
0
20
15
10
5
0
350
250
150
2100
2000
1900
4/15
4/29
5/13
5/27
6/10
6/24
7/8
7/22
8/5
8/19

510 Figure 4

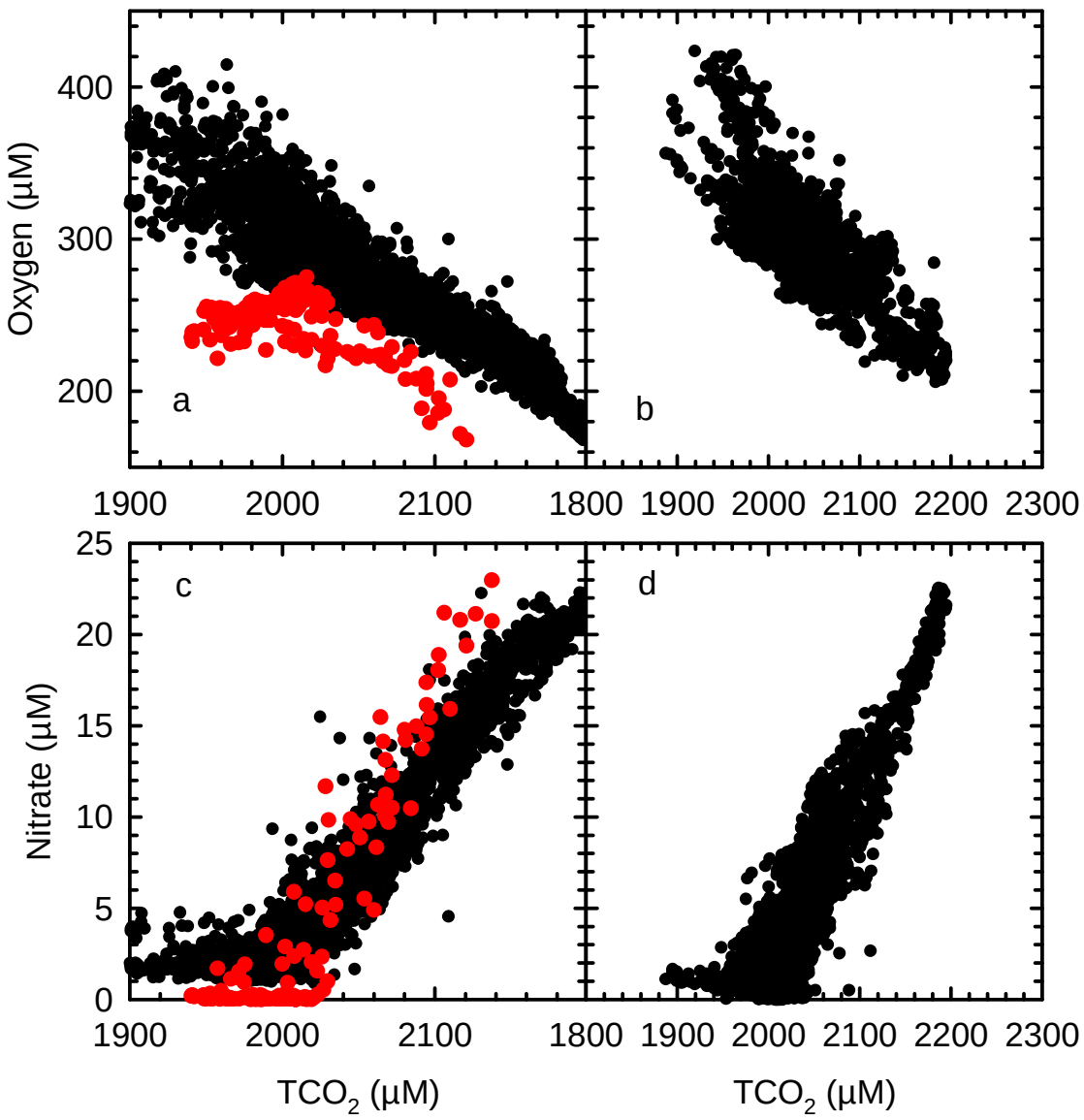
Oxygen (µM)
400
300
200
a
b
1900
2000
2100
1800
1900
2000
2100
2200
2300
Nitrate (µM)
25
20
15
10
5
0
c
d
TCO2 (µM)
TCO2 (µM)

514 Figure 5

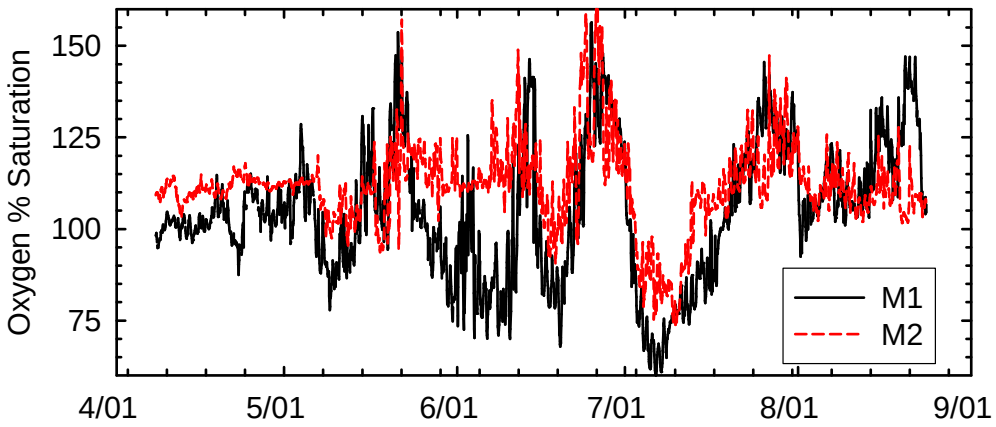

515 Figure 6

516

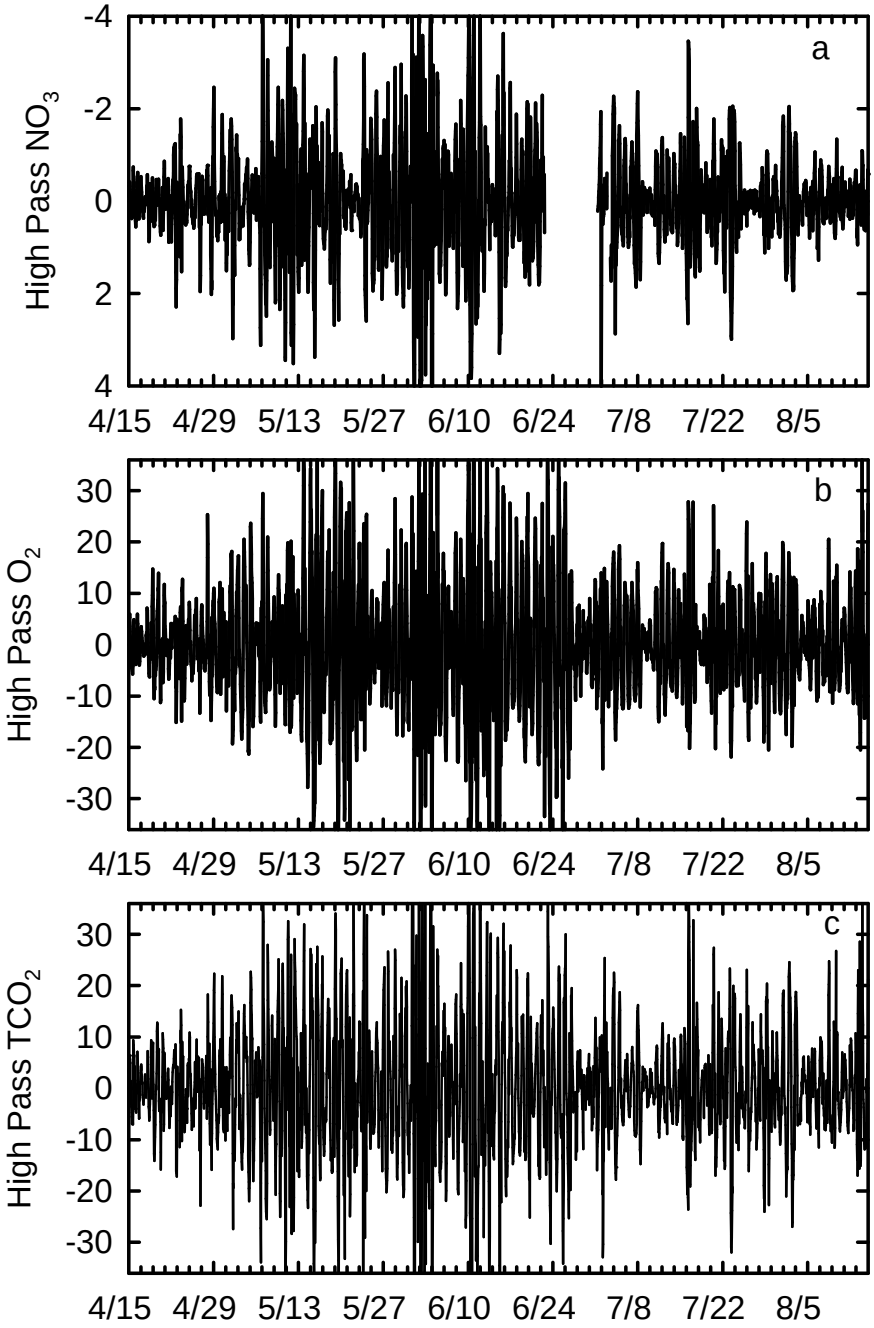

517 Figure 7

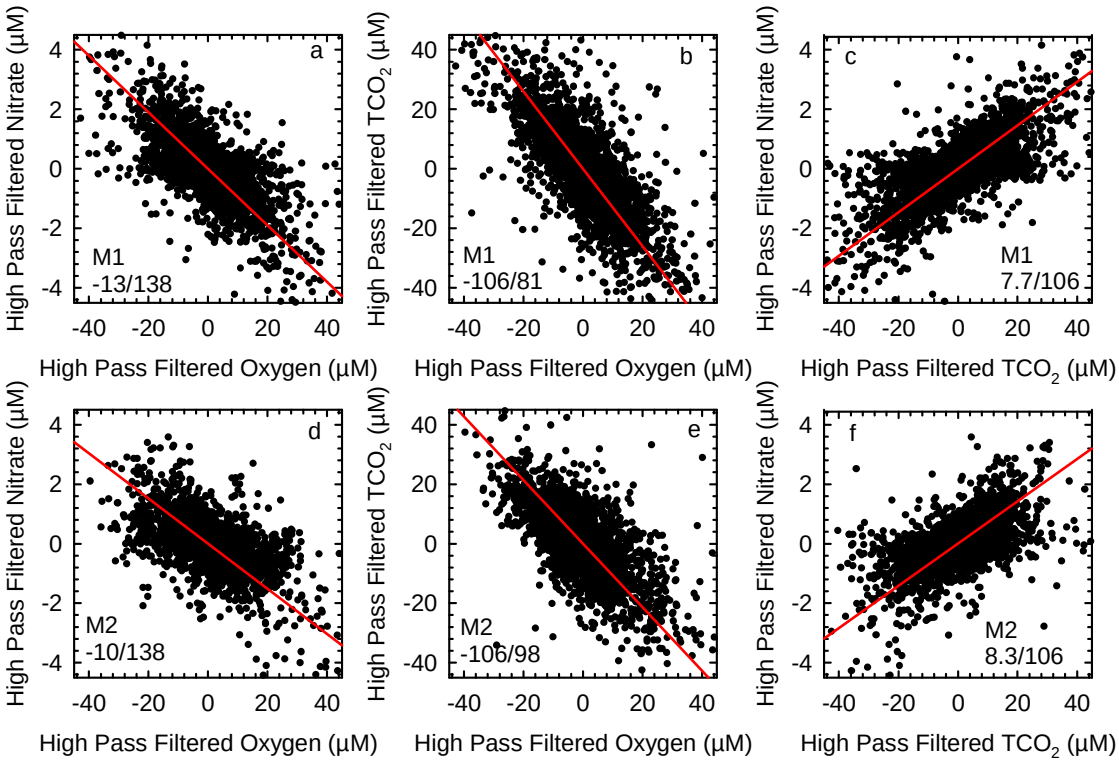

518

519 Fig. 8

520

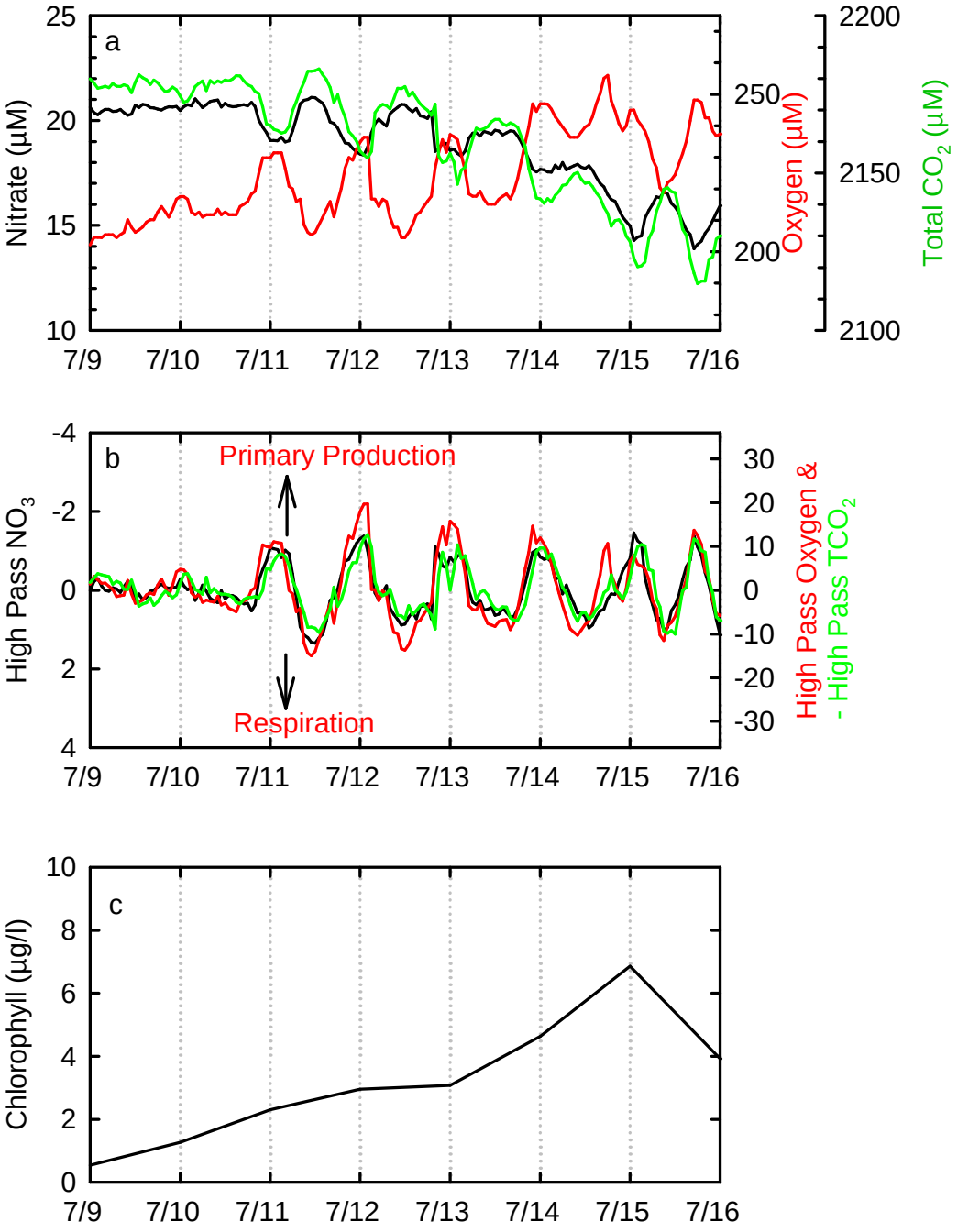
a
Nitrate (µM)
Oxygen (µM)
Total CO2 (µM)
25
20
15
10
250
200
2200
2150
2100
7/9
7/10
7/11
7/12
7/13
7/14
7/15
7/16
b
Primary Production
Respiration
High Pass NO3
High Pass Oxygen &
- High Pass TCO2
-4
-2
0
2
4
30
20
10
0
-10
-20
-30
c
Chlorophyll (µg/l)
10
8
6
4
2
0

521 Figure 9

522

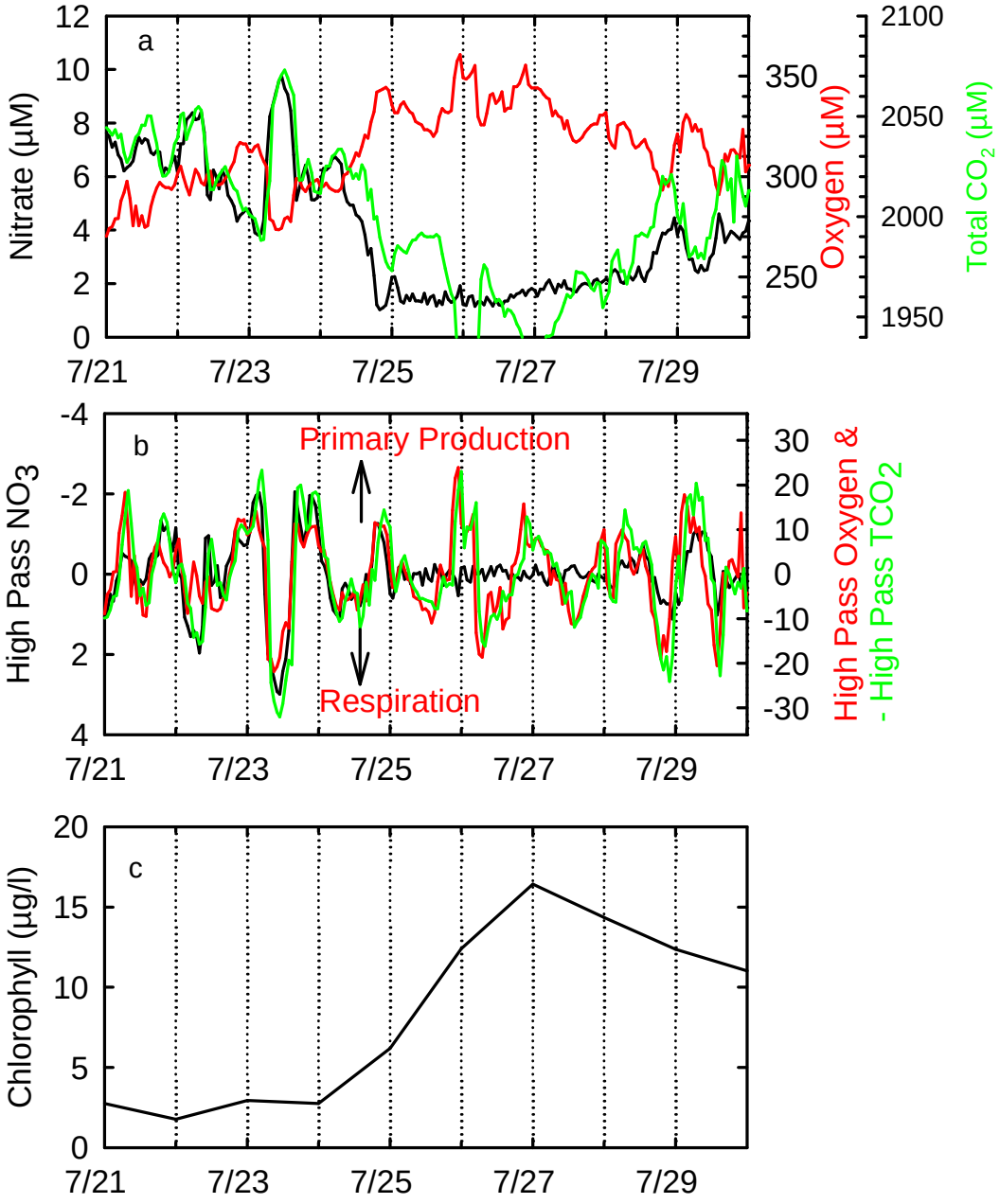

523 Figure 10

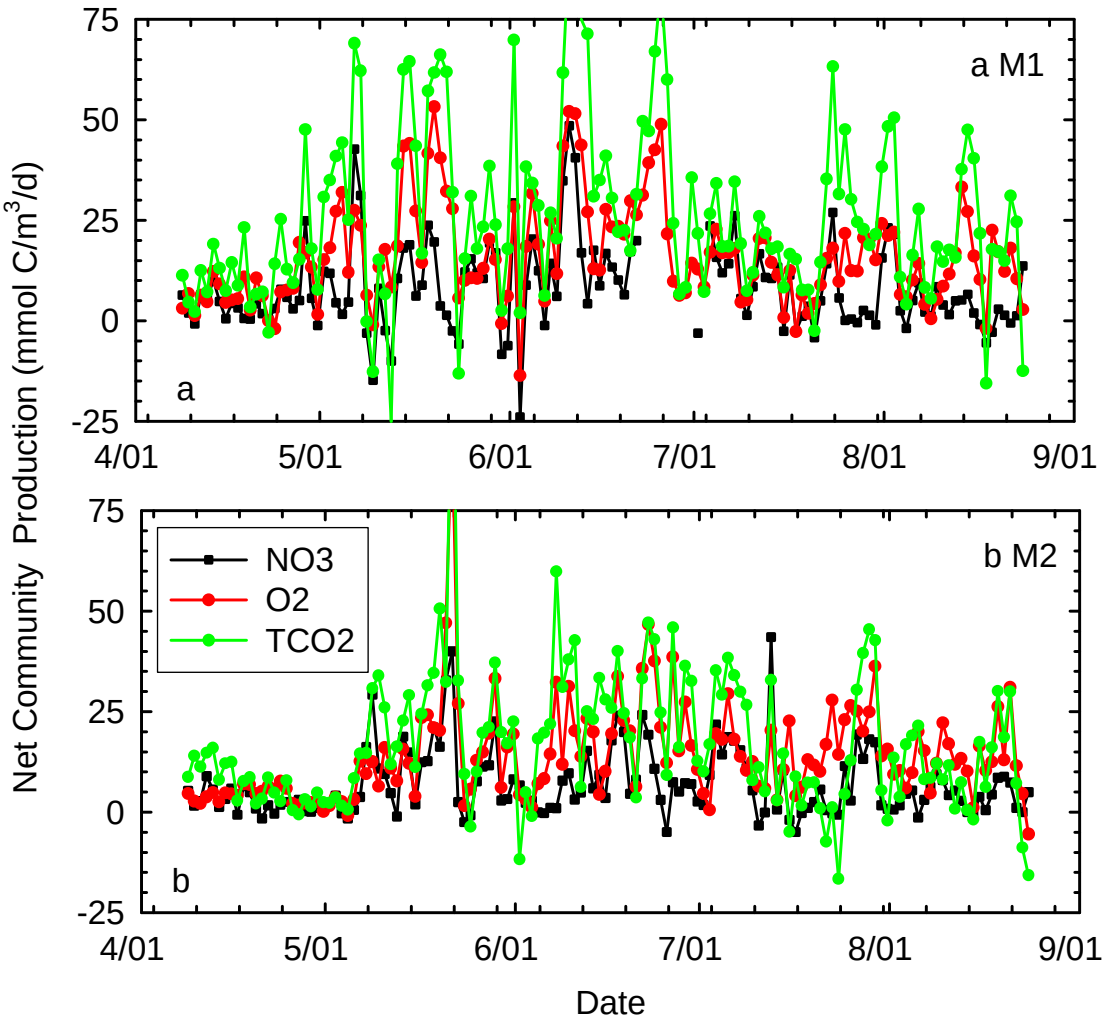

524 Fig. 11

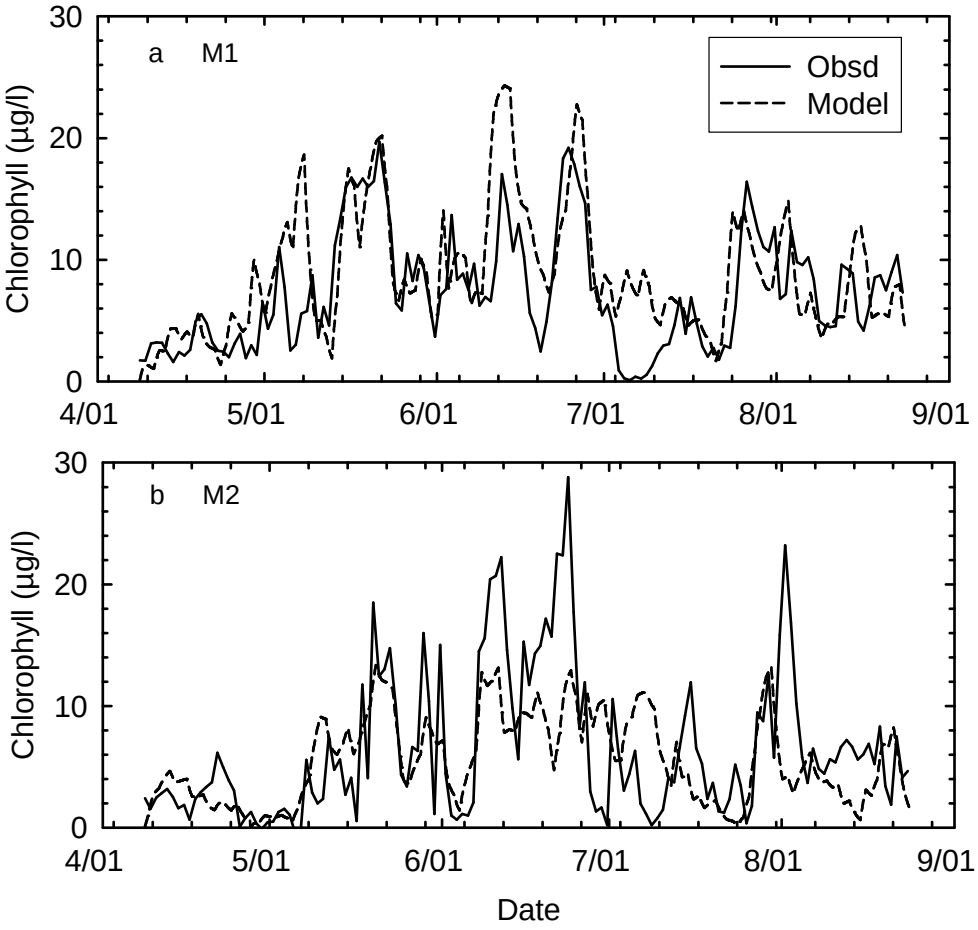
a M1
Obsd
Model
Chlorophyll (µg/l)
30
20
10
0
4/01
5/01
6/01
7/01
8/01
9/01
b M2
Chlorophyll (µg/l)
Date

525 Fig. 12

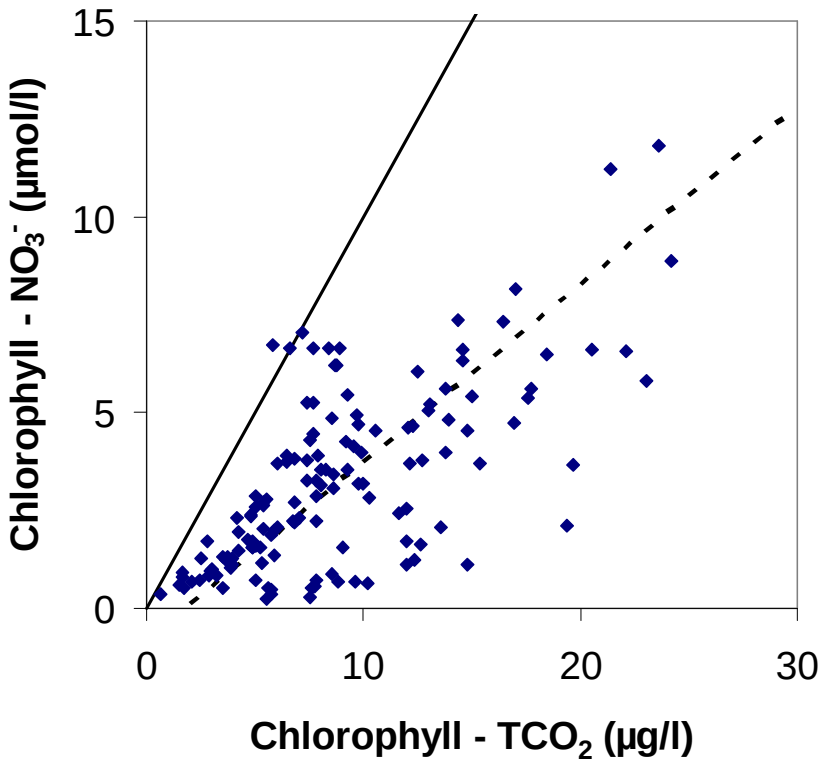
15
10
5
0
0
10
20
30
Chlorophyll - NO_3^- (µmol/l)
Chlorophyll - TCO_2 (µg/l)

526 Figure 13

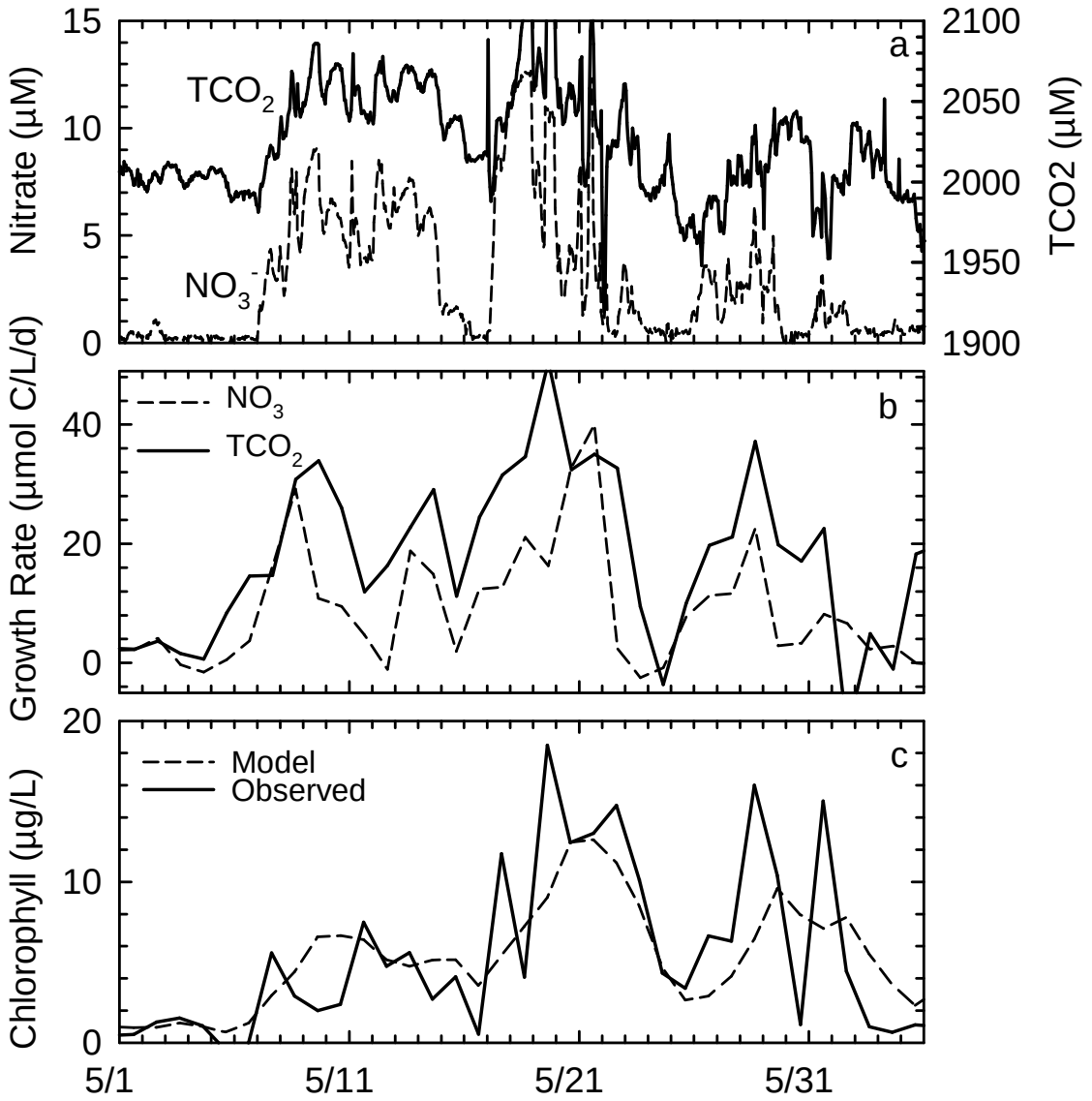

527 Fig. 14

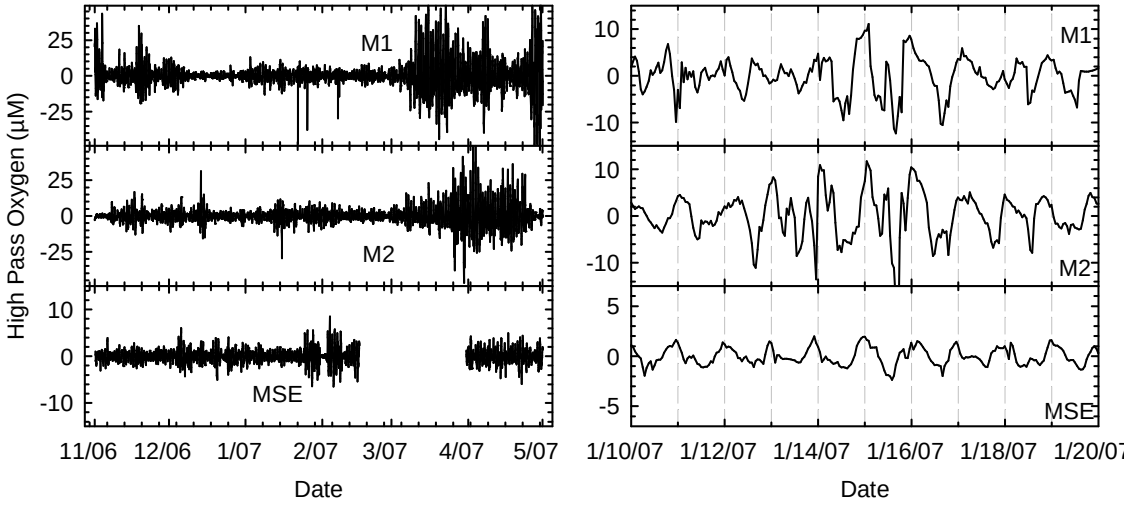
High Pass Oxygen (µM)
25
0
-25
M1
25
0
-25
M2
10
0
-10
MSE
11/06
12/06
1/07
2/07
3/07
4/07
5/07
Date
10
0
-10
M1
10
0
-10
M2
5
0
-5
MSE
1/10/07
1/12/07
1/14/07
1/16/07
1/18/07
1/20/07
Date

528 Fig. 15

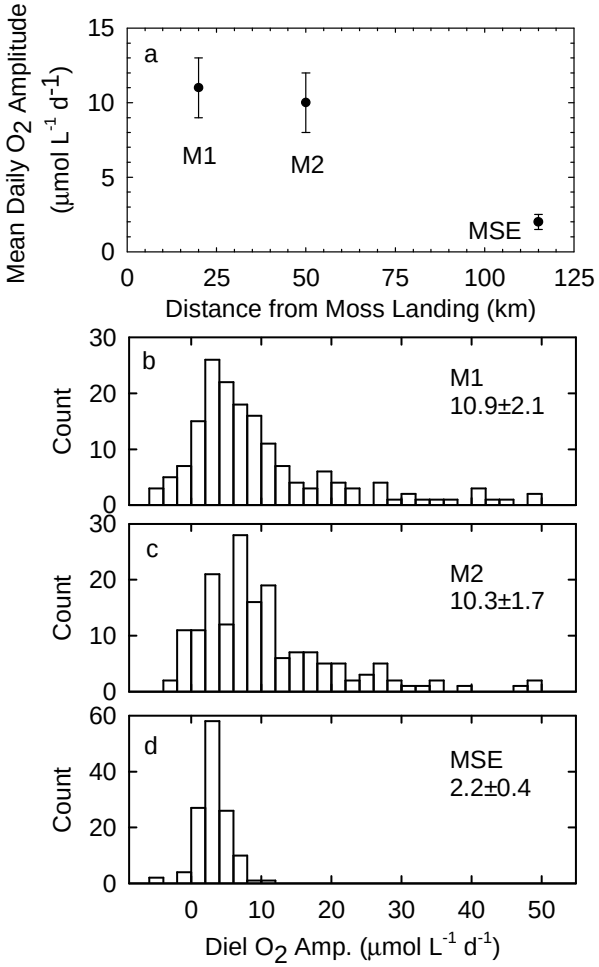
a
M1
M2
MSE
Mean Daily O2 Amplitude (µmol L-1 d-1)
Distance from Moss Landing (km)
b
M1
10.9±2.1
c
M2
10.3±1.7
d
MSE
2.2±0.4
Count
Diel O2 Amp. (µmol L-1 d-1)